Moving Boundary-Moving Mesh Analysis of Freezing Process in Water-Saturated Porous Media Using a Combined Transfinite Interpolation and PDE Mapping Methods

P. Rattanadecho[1]
Faculty of Engineering,
Thammasat University (Rangsit Campus),
Pathumthani 12121, Thailand
e-mail: ratphadu@engr.tu.ac.th

S. Wongwises
Department of Mechanical Engineering,
King Mongkut's University of Technology
Thonburi,
91 Suksawas 48,
Rasburana, Bangkok 10140, Thailand

This paper couples the grid generation algorithm with the heat transport equations and applies them to simulate the thermal behavior of freezing process in water-saturated porous media. Focus is placed on establishing a computationally efficient approach for solving moving boundary heat transfer problem, in two-dimensional structured grids, with specific application to an undirectional solidification problem. Preliminary grids are first generated by an algebraic method, based on a transfinite interpolation method, with subsequent refinement using a partial differential equation (PDE) mapping (parabolic grid generation) method. A preliminary case study indicates successful implementation of the numerical procedure. A two-dimensional solidification model is then validated against available analytical solution and experimental results and subsequently used as a tool for efficient computational prototyping. The results of the problem are in good agreement with available analytical solution and experimental results.
[DOI: 10.1115/1.2780177]

Keywords: solidification, transfinite interpolation, PDE mapping, moving boundary

Introduction

Transient heat transfer problems involving solidification or melting processes generally refer to as "moving boundary" or "phase change." Solidification and melting are important parts of manufacturing processes such as crystal growth, casting, welding, coating process, thermal energy storage, aerodynamic ablation, pipeline transport in permafrost regions, and cryosurgery and in the transportation of coal in coal weather, thermal energy storage, ice accretion on vehicles and static structures, solidification of alloys, food processing, freeze drying, chemical processes, and cryopreservation of engineering tissues. In all these processes, phase changes of material are caused by the heat transfer to and from both of the phases on either side of the interface. This yields melting if the net heat is added to the solid part of the interface and solidification when the net heat is subtracted.

Up to the present time, the related problems of solidification process in 1D have been investigated both experimentally and numerically by many researchers and up to date reviews are available; Landua [1], Murray and Landis [2], Frivik and Comini [3], Sparrow and Broadbent [4], Voller and Cross [5], Weaver and Viskanta [6], Chellaiah and Viskanta [7], Hasan et al. [8], Charn-Jung and Kaviany [9], Rattanadecho [10,11], Pak and Plumb [12], Hao and Tao [13], Attinger and Poulikakos [14], Jiang et al. [15], Hao and Tao [16], Elgafy et al. [17], and Ayasoufi et al. [18]. Regarding specific analysis to moving boundary problems, in a 2D or 3D, there have been significant research studies executed in the recent past including Lynch [19], Cao et al. [20], Chatterjee and Prasad [21], Duda et al. [22], Saitoh [23], Gong and Mujumdar [24], and Beckett et al. [25].

When solving a moving boundary problem, complication arises because the interface between the solid and liquid phases is moving as the latent heat is absorbed or released at the interface. As such, the position of the interface is not known a priori and the domains over which the energy equations are solved vary. Also, physical quantities such as enthalpy and transport properties vary discontinuously across these interfaces. Therefore, solutions to moving boundary problems, especially for multidimensional domains, should cope with difficulties associated with the nonlinearity in the interfacial conditions and unknown positions of arbitrary interfaces. Moreover, in numerical approximations of this problem with discontinuous coefficients, often the largest numerical errors are introduced in a neighborhood of the discontinuities. These errors are often greatly reduced if the grid generation and solution procedure are separated with the discontinuities and special formulas are used to incorporate the jump conditions directly into the numerical model.

It is well known that the construction itself of a coordinate grid in a specified domain is not a trivial matter and the numerical solution of the governing partial differential equations upon it is indeed a formidable computational task, which in turn puts a high premium on grid generator that can provide an optimum resolution with an economy of nodal points. It is found that these two items, grid generation and solution procedure, are separate and distinct operations, and as such should be treated in an independent and modular way. The means for grid generation should not be dictated by the limitations of a given specific flow solution procedure and conversely the method that determines the flow should accept as input an arbitrary set of coordinate points, which constitutes the grid. In general, of course, these two operations

[1]Corresponding author.

Contributed by the Heat Transfer Division of ASME for publication in the JOURNAL OF HEAT TRANSFER. Manuscript received June 14, 2006; final manuscript received April 20, 2007; published online January 25, 2008. Review conducted by Jose L. Lage.

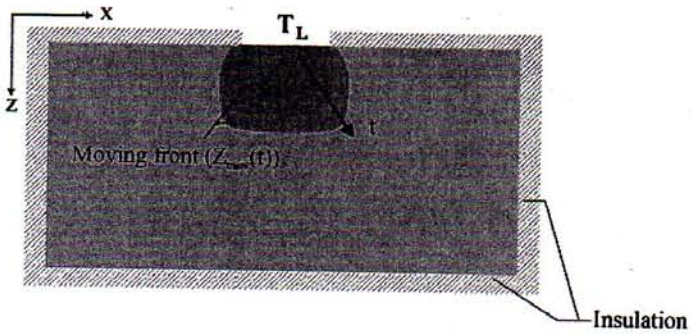

Fig. 1 Physical model

can never be totally independent because the logistic structure of the information, the location of outer boundaries, the nature of coordinate, and the types of grid singularities are items that have to be closely coordinated between the flow solver and the grid generator (Eriksson [26]). Grid generation for multidimensional geometries using transfinite interpolation functions was studied by Coons [27], Cook [28], and Gordon and Hall [29]. Ettouney and Brown [30] successfully modeled slightly nonplanar interfaces by using an algebraic grid generation system where the interface was described in terms of univariate function.

Although grid generation is the heart of most numerical algorithms for flow problems or nonphase change problem, little effort has been reported on phase change problems, particularly the problem that is to couple the grid generation algorithm with the heat transport equations.

This paper deals with thermodynamically consistent numerical predictions of freezing process of water in a rectangular cavity filled with a porous medium subjected to a constant temperature heat sink using moving grids. They will also permit a continuous determination of the undirectional freezing front move and indicate the internal temperature distribution with a greater degree of boundary complexity and offer the highest overall accuracies and smooth grid point distribution. Numerically, for generating a boundary/interface fitted coordinate system, structured grids are initialized using transfinite interpolation algebraic methods and the quality of structured grids can be significantly improved by applying parabolic-partial differential equation (PDE) methods. These methods iteratively solve unsteady conduction's equation together with moving boundary condition considering conduction as the only mode of heat transfer.

Analysis of Heat Transport and Freezing Front

The two-dimensional system illustrated schematically in Fig. 1 is considered. Initially, the walls are all insulated and the rectangular cavity is filled with a porous medium (PM) consisting of the glass beads and phase change material (PCM) in the liquid state (water), both at the fusion temperature T_f. At time, $t>0$, a strip of isothermal surface, T_L, less than the fusion temperature is imposed on the partial top wall. Freezing is initiated at this partial wall and the freezing interface moves from top to bottom.

Assumptions. In order to analyze the process of heat transport due to freezing of water in a rectangular cavity filled with a PM subjected to a constant temperature heat sink, we introduce the following assumptions:

(1) The temperature field can be assumed to be two dimensional.
(2) The thermal equilibrium exists between PCM and PM; this is possible when the porous matrix has a little larger thermal conductivity than the PCM, and the interphase heat transfer can be properly neglected.
(3) Properties of PM are isotropic.
(4) The volumetric change due to solidification is negligible.
(5) The effect of the natural convection in liquid is negligible.

Table 1 Thermal properties of the unfrozen layer and frozen layer

Properties	Unfrozen layer	Frozen layer
ρ (kg/m^3)	1942.0	1910.0
a (m^2/s)	0.210×10^{-6}	0.605×10^{-6}
λ (W/m K)	0.855	1.480
c_p (J/kg K)	2.099×10^{3}	1.281×10^{3}

Basic Equations. The applicable differential equation for two-dimensional heat flow with averaged thermal properties in both the unfrozen and frozen layers, are, respectively,

$$\frac{\partial T_l}{\partial t}=a_l\left(\frac{\partial^2 T_l}{\partial x^2}+\frac{\partial^2 T_l}{\partial z^2}\right) \tag{1}$$

$$\frac{\partial T_s}{\partial t}=a_s\left(\frac{\partial^2 T_s}{\partial x^2}+\frac{\partial^2 T_s}{\partial z^2}\right) \tag{2}$$

After some mathematical manipulations, a transformation model of the original governing differential equations becomes [2]

$$\frac{\partial T_l}{\partial t}=a_l\left(\frac{\partial^2 T_l}{\partial x^2}+\frac{\partial^2 T_l}{\partial z^2}\right)+\left(\frac{\partial T_l}{\partial z}\right)\frac{dz}{dt} \tag{3}$$

$$\frac{\partial T_s}{\partial t}=a_s\left(\frac{\partial^2 T_s}{\partial x^2}+\frac{\partial^2 T_s}{\partial z^2}\right)+\left(\frac{\partial T_s}{\partial z}\right)\frac{dz}{dt} \tag{4}$$

where the last terms of Eqs. (3) and (4) result from a coordinate transformation attached to the moving boundary. In the unfrozen layer, if internal natural convection can be neglected because the presence of glass beads minimizes the effect of natural convection current.

Treatment of the Moving Boundary. A consideration of the energy balance at the interface between the unfrozen layer and frozen layer provides the following equation (moving boundary or Stefan condition):

$$\left(\lambda_s\frac{\partial T_s}{\partial z}-\lambda_l\frac{\partial T_l}{\partial z}\right)\left[1+\left(\frac{\partial z_{\text{mov}}}{\partial x}\right)^2\right]=\rho_s L_s\frac{\partial z_{\text{mov}}}{\partial t} \tag{5}$$

where $\partial z_{\text{mov}}/\partial t$ is the velocity of fusion front or freezing front, and L_s the latent heat of fusion. To avoid changes in the physical dimensions as the freezing front progresses, $\rho_s=\rho_l$ will be specified. In this study, the thermal conductivity, λ_l and λ_s, are bulk-average values for the glass beads and the water or ice, respectively (refer to Table 1).

Boundary Conditions. Subject to appropriate initial condition and the boundary conditions are as follows:

(a) *The localized freezing condition.* The constant temperature heat sink is imposed on the partial top wall:

$$T=T_L \tag{6}$$

(b) *Adiabatic condition.* The walls except the position of localized heating condition are all insulated:

$$\frac{\partial T}{\partial x}=\frac{\partial T}{\partial z}=0 \tag{7}$$

Grid Generation by Transfinite Interpolation and PDE Mapping

Generally, two types of structured grid generation are in use: algebraic method, i.e., transfinite interpolation and PDE methods. Transfinite interpolation method provides a relatively easy way of obtaining an initial grid that can be refined and smoothed by other techniques, whether algebraic, PDE method. For more complex

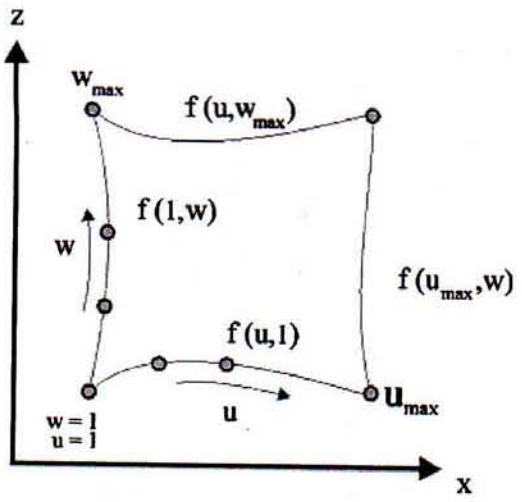

Fig. 2 The parametric domain with $f_{(u,w)}$ specified on planes of constant u, w

geometries, such as this work, it is preferable to construct grid initially by transfinite interpolation and to refine the grid filled in Cartesian coordinates in the interior of a domain by parabolic-PDE method subsequently.

Transfinite Interpolation. The present method of constructing a two-dimensional boundary-conforming grid for a freezing sample is a direct algebraic approach based on the concept of transfinite interpolation. In this method, no partial differential equations are solved to obtain the curvilinear coordinates, and the same system is used for the entire domain. The algebraic method can be easier to construct than PDE mapping methods and give easier control over grid characteristics, such as orthogonality and grid point spacing. However, this method is sometime criticized for allowing discontinuities on the boundary to propagate into the interior and for not generating grids as smooth as those generated by the PDE mapping method. The main idea behind this work, prior to generation of grids by PDE mapping methods, it is preferable to obtain first preliminary grids using the algebraic method, i.e., transfinite interpolation method. The combined transfinite interpolation and PDE mapping methods are used to achieve a very smoother grid point distribution and boundary point discontinuities are smoothed out in the interior domain.

For the concept of transfinite interpolation method, a significant extension of the original formulation by Gordon and Hall [29] have made it possible to initially generate global grid system with geometry specifications only on the outer boundaries of the computation domain and yet obtain a high degree of local control. Moreover, to successfully track the moving boundary front, the grid generation mapping must adapt to large deformations of the interface shape while maintaining as much orthogonality and smoothness as possible. Due to the generality of the method, it has been possible to use more advanced mappings than conventional types and thereby improve the overall efficiency of the grid in terms of computational work for a given resolution.

In Fig. 2, the present method of constructing a two-dimensional boundary-conforming grid for a sample is a direct algebraic approach based on the concept of transfinite or multivariate interpolation. It is possible to initially generate global single plane transformations with geometry specifications only on outer boundaries of the computational domain.

Let $f(u,w)=[x(u,w),z(u,w)]$ denote a vector-valued function of two parameters u, w defined on the region $u_1 \leqslant u \leqslant u_{max}$, $w_1 \leqslant w \leqslant u_{max}$. This function is not known throughout the region, only on certain planes (Fig. 2).

The transfinite interpolation procedure then gives the interpolation function $f_{(u,w)}$ by the recursive algorithm:

$$f^{(1)}_{(u,w)} = A_{1(u)} f_{(1,w)} + A_{2(u)} f_{(u_{max},w)}$$

$$f_{(u,w)} = f^{(1)}_{(u,w)} + B_{1(w)}[f_{(u,1)} - f^{(1)}_{(u,1)}] + B_{2(w)}[f_{(u,w_{max})} - f^{(1)}_{(u,w_{max})}] \tag{8}$$

where $A_{1(u)}, A_{2(u)}, B_{1(w)}$, and $B_{2(w)}$ defined the set of univariate blending functions, which only have to satisfy the following conditions:

$$A_{1(1)} = 1 \quad A_{1(u_{max})} = 0$$

$$A_{2(1)} = 0 \quad A_{2(u_{max})} = 1$$

$$B_{1(1)} = 1 \quad B_{1(w_{max})} = 0$$

$$B_{2(1)} = 0 \quad B_{2(w_{max})} = 1$$

Further, the general form in algebraic equations can be defined as

$$A_{1(u)} = \frac{u_{max} - u}{u_{max} - 1} \quad A_{2(u)} = 1 - A_{1(u)}$$

$$B_{1(w)} = \frac{w_{max} - w}{w_{max} - 1} \quad B_{2(w)} = 1 - B_{1(w)} \tag{9}$$

The grid motion defined from a moving boundary motion is modeled using a Stefan equation (Eq. (13)) with a transfinite mapping method.

PDE Mapping. In the proposed grid generation mapping, all grids discussed and displayed have been couched in terms of finite difference algorithm applications, with the understanding that whatever nonuniform grid exists in the physical space, there exists a transformation which will recast it as a uniform rectangular grid in the computational space. The implicit-finite difference calculations are then made over this uniform grid in the computational space, after which the field results are transferred directly back to the corresponding points in the physical space. The purpose of generating a smooth grid that conforms to physical boundaries of problem is, of course, to solve the partial differential equations specified in the problem by finite difference scheme, capable of handling general nonorthogonal curvilinear coordinates.

Corresponding to Fig. 1, as freezing proceeds, a freezing front denoted here z_{mov} is formed. Due to the existence of this freezing front, the frozen (ice) and unfrozen (water) domains are irregular and time dependent. To avoid this difficulty, a curvilinear system of coordinates is used to transform the physical domain into rectangular region for the computational domain.

It is convenient to introduce a general curvilinear coordinate system as follows (Anderson [31]):

$$x = x(\xi,\eta) \quad z = z(\xi,\eta) \text{ or } \xi = \xi(x,z) \quad \eta = \eta(x,z) \tag{10}$$

The moving boundaries are immobilized in the dimensionless (ξ,η) coordinate for all times. With the details omitted, then the transformation of Eqs. (3) and (5) can be written, respectively, as:

$$\frac{\partial T_l}{\partial t} = \frac{a_l}{J^2}\left(\alpha\frac{\partial^2 T_l}{\partial \xi^2} - 2\beta\frac{\partial^2 T_l}{\partial \xi \partial \eta} + \gamma\frac{\partial^2 T_l}{\partial \eta^2}\right) + \frac{a_l}{J^3}\left[\left(\alpha\frac{\partial^2 x}{\partial \xi^2}\right)\left(z_\xi\frac{\partial T_l}{\partial \eta} - z_\eta\frac{\partial T_l}{\partial \xi}\right) + \alpha\frac{\partial^2 z}{\partial \xi^2} - 2\beta\frac{\partial^2 z}{\partial \xi \partial \eta} + \gamma\frac{\partial^2 z}{\partial \eta^2}\left(-x_\xi\frac{\partial T_l}{\partial \eta}\right)\right] + \frac{1}{J}\left(x_\xi\frac{\partial T_l}{\partial \eta}\right)\frac{dz}{dt} \tag{11}$$

$$\frac{\partial T_s}{\partial t}=\frac{a_s}{J^2}\left(\alpha\frac{\partial^2 T_s}{\partial\xi^2}-2\beta\frac{\partial^2 T_s}{\partial\xi\partial\eta}+\gamma\frac{\partial^2 T_s}{\partial\eta^2}\right)+\frac{a_s}{J^3}\left[\left(\alpha\frac{\partial^2 x}{\partial\xi^2}\right)\left(z_\xi\frac{\partial T_s}{\partial\eta}-z_\eta\frac{\partial T_s}{\partial\xi}\right)+\alpha\frac{\partial^2 z}{\partial\xi^2}-2\beta\frac{\partial^2 z}{\partial\xi\partial\eta}+\gamma\frac{\partial^2 z}{\partial\eta^2}\left(-x_\xi\frac{\partial T_s}{\partial\eta}\right)\right]+\frac{1}{J}\left(x_\xi\frac{\partial T_s}{\partial\eta}\right)\frac{dz}{dt} \tag{12}$$

$$\left[\lambda_s\frac{1}{J}\left(x_\xi\frac{\partial T_s}{\partial\eta}\right)-\lambda_l\frac{1}{J}\left(x_\xi\frac{\partial T_l}{\partial\eta}\right)\right]\left\{1+\left[\frac{1}{J}\left(z_\eta\frac{\partial z_{\mathrm{mov}}}{\partial\xi}-z_\xi\frac{\partial z_{\mathrm{mov}}}{\partial\eta}\right)\right]^2\right\}=\rho_s L_s\frac{\partial z_{\mathrm{mov}}}{\partial t} \tag{13}$$

where $J=x_\xi z_\eta-x_\eta z_\xi$, $\alpha=x_\eta^2+z_\eta^2$, $\beta=x_\xi x_\eta+z_\xi z_\eta$, $\gamma=x_\xi^2+z_\xi^2$ and x_ξ, x_η, z_ξ, and z_η denote partial derivatives, J is the Jacobian, β,α,γ are the geometric factors, and η,ξ are the transformed coordinates.

Solution Method

In order to initiate numerical simulation, a very thin layer of freeze with a constant thickness $z_{\mathrm{mov}(0)}$ was assumed to be present. This initial condition is obtained from the Stefan solution in the freeze and a linear temperature distribution in the frozen layer. Tests revealed that the influence of $z_{\mathrm{mov}(0)}$ could be neglected as $z_{\mathrm{mov}(0)}$ was sufficiently small.

The transient heat equations (Eqs. (11) and (12)) and the Stefan equation (Eq. (13)) are solved by using implicit-finite difference method. A system of nonlinear equations results whereby each equation for the internal nodes can be cast into a numerical discretization.

In transient heat equation for unfrozen layer,

$$\begin{aligned}T_l^{n+1}(k,i)=&\left(\frac{1}{1+\frac{2a_l\Delta t}{J^2(k,i)}\{[\alpha(k,i)/\Delta\zeta\Delta\zeta]+[\gamma(k,i)/\Delta\eta\Delta\eta]\}}\right)\left(T_l^n(k,i)+\frac{a_l\Delta t}{J^2(k,i)}\left[\alpha(k,i)\frac{T_l^{n-1}(k,i+1)+T_l^{n+1}(k,i-1)}{\Delta\zeta\Delta\zeta}\right]-2\beta(k,i)\right.\\&\times\left\{\left[\frac{T_l^{n-1}(k+1,i+1)-T_l^{n+1}(k-1,i+1)}{2\Delta\eta}-\frac{T_l^{n-1}(k+1,i-1)-T_l^{n+1}(k-1,i-1)}{2\Delta\zeta}\right]\right\}\Big/2\Delta\zeta+\gamma(k,i)\\&\times\left.\left[\frac{T_l^{n-1}(k+1,i)+T_l^{n+1}(k-1,i)}{\Delta\eta\Delta\eta}\right]\right)+\frac{a_l\Delta t}{J^3(k,i)}\left(\left[\alpha(k,i)\frac{X(k,i+1)-2X(k,i)+X(k,i-1)}{\Delta\zeta\Delta\zeta}\right]\left\{\left[\frac{Z(k,i+1)-Z(k,i-1)}{2\Delta\zeta}\right]\right.\right.\\&\times\left[\frac{T_l^{n-1}(k+1,i)-T_l^{n+1}(k-1,i)}{2\Delta\eta}\right]-\left[\frac{Z(k+1,i)-Z(k-1,i)}{2\Delta\eta}\right]\left[\frac{T_l^{n-1}(k,i+1)-T_l^{n+1}(k,i-1)}{2\Delta\zeta}\right]\Big\}+\alpha(k,i)\\&\times\left[\frac{Z(k,i+1)-2Z(k,i)+Z(k,i-1)}{\Delta\zeta\Delta\zeta}\right]-2\beta(k,i)\left\{\left[\frac{Z(k+1,i+1)-Z(k-1,i+1)}{2\Delta\eta}\right]\right.\\&\left.-\left[\frac{Z(k+1,i-1)-Z(k-1,i-1)}{2\Delta\eta}\right]\right\}\Big/2\Delta\zeta+\gamma(k,i)\left[\frac{Z(k+1,i)-2Z(k,i)+Z(k-1,i)}{\Delta\eta\Delta\eta}\right]*\left\{-\frac{[X(k,i+1)-X(k,i-1)]}{2\Delta\zeta}\right\}\\&\times\left.\left[\frac{T_l^n(k+1,i)-T_l^n(k-1,i)}{2\Delta\eta}\right]+\frac{1}{J(k,i)}\left[\frac{X(k,i+1)-X(k,i-1)}{2\Delta\zeta}\right]\left[\frac{T_l^n(k+1,i)-T_l^n(k-1,i)}{2\Delta\eta}\right]dz(k,i)\right)\end{aligned} \tag{14}$$

In transient heat equation for frozen layer,

$$\begin{aligned}T_s^{n+1}(k,i)=&\left(\frac{1}{1+[2a_l\Delta t/J^2(k,i)]\{[\alpha(k,i)/\Delta\zeta\Delta\zeta]+[\gamma(k,i)/\Delta\eta\Delta\eta]\}}\right)\left(T_s^n(k,i)+\frac{a_l\Delta t}{J^2(k,i)}\left[\alpha(k,i)\frac{T_s^{n-1}(k,i+1)+T_s^{n+1}(k,i-1)}{\Delta\zeta\Delta\zeta}\right]-2\beta(k,i)\right.\\&\times\left\{\left[\frac{T_s^{n-1}(k+1,i+1)-T_s^{n+1}(k-1,i+1)}{2\Delta\eta}-\frac{T_s^{n-1}(k+1,i-1)-T_s^{n+1}(k-1,i-1)}{2\Delta\zeta}\right]\right\}\Big/2\Delta\zeta+\gamma(k,i)\\&\times\left.\left[\frac{T_s^{n-1}(k+1,i)+T_s^{n+1}(k-1,i)}{\Delta\eta\Delta\eta}\right]\right)+\frac{a_l\Delta t}{J^3(k,i)}\left(\left[\alpha(k,i)\frac{X(k,i+1)-2X(k,i)+X(k,i-1)}{\Delta\zeta\Delta\zeta}\right]\left\{\left[\frac{Z(k,i+1)-Z(k,i-1)}{2\Delta\zeta}\right]\right.\right.\\&\times\left[\frac{T_s^{n-1}(k+1,i)-T_s^{n+1}(k-1,i)}{2\Delta\eta}\right]-\left[\frac{Z(k+1,i)-Z(k-1,i)}{2\Delta\eta}\right]\left[\frac{T_s^{n-1}(k,i+1)-T_s^{n+1}(k,i-1)}{2\Delta\zeta}\right]\Big\}+\alpha(k,i)\\&\times\left[\frac{Z(k,i+1)-2Z(k,i)+Z(k,i-1)}{\Delta\zeta\Delta\zeta}\right]-2\beta(k,i)\left\{\left[\frac{Z(k+1,i+1)-Z(k-1,i+1)}{2\Delta\eta}\right]\right.\\&\left.-\left[\frac{Z(k+1,i-1)-Z(k-1,i-1)}{2\Delta\eta}\right]\right\}\Big/2\Delta\zeta+\gamma(k,i)\left[\frac{Z(k+1,i)-2Z(k,i)+Z(k-1,i)}{\Delta\eta\Delta\eta}\right]\left\{-\frac{[X(k,i+1)-X(k,i-1)]}{2\Delta\zeta}\right\}\\&\times\left.\left[\frac{T_s^n(k+1,i)-T_s^n(k-1,i)}{2\Delta\eta}\right]+\frac{1}{J(k,i)}\left[\frac{X(k,i+1)-X(k,i-1)}{2\Delta\zeta}\right]\left[\frac{T_s^n(k+1,i)-T_s^n(k-1,i)}{2\Delta\eta}\right]*dz(k,i)\right)\end{aligned} \tag{15}$$

In Stefan condition,

$$Z^{n+1}(k,i) = Z^n(k,i) + \frac{\Delta T}{\rho_s L_s}\left[\left\{\frac{\lambda_s}{J(k-1,i)} * \left[\frac{X(k-1,i+1)-X(k-1,i-1)}{2\Delta\zeta}\right]\left[\frac{3T(k,i)-4T(k-1,i)+T(k-2,i)}{2\Delta\eta}\right]\right.\right.$$
$$\left. - \frac{\lambda_l}{J(k+1,i)} * \left[\frac{X(k+1,i+1)-X(k+1,i-1)}{2\Delta\zeta}\right]\left[\frac{-3T(k,i)+4T(k+1,i)-T(k+2,i)}{2\Delta\eta}\right]\right\}\left(1+\left\{\left[\frac{Z^n(k+1,i)-Z^n(k-1,i)}{2\Delta\eta}\right]\right.\right.$$
$$\left.\left.\times\left[\frac{Z^n(k+1,i)-Z^n(k-1,i)}{2\Delta\zeta}\right] - \left[\frac{Z^n(k,i+1)-Z^n(k,i-1)}{2\Delta\zeta}\right]\left[\frac{Z^n(k,i+1)-Z^n(k,i-1)}{2\Delta\eta}\right]\right\}^2\right)\right] \quad (16)$$

The details of computational schemes and strategy for solving the combined transfinite interpolation functions (Eqs. (8) and (9)) and PDE mapping (Eqs. (14)–(16)) are illustrated in Fig. 3.

The calculation conditions were as follows:

(1) The time step of dt=1 s is used for the computation of temperature field and location of freezing front.
(2) Number of grid: N=100(length)×100(height).
(3) Relative errors in the iteration procedure of 10^{-8} were chosen.

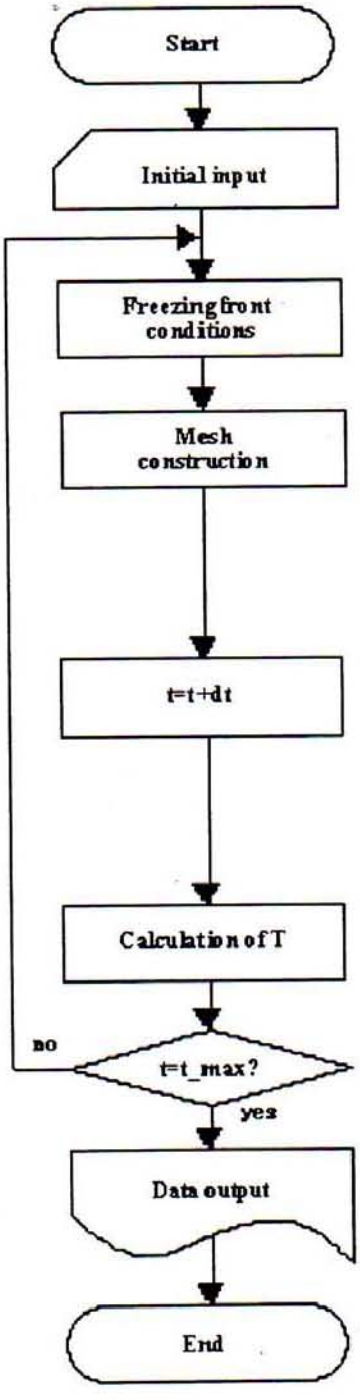

Fig. 3 Strategy for calculation

Experiment

The freezing experiments are performed in a rectangular test cell filled with a PM (porosity, ϕ=0.4) with inside dimensions of 10 cm in length (x), 5 cm in height (z), and 2.5 cm in depth (y). The partial horizontal top wall and bottom wall and the vertical front and back walls are made of acrylic resin with a thickness of 3 mm. The entire test cell is covered with 8 cm thick Styrofoam on all sides to minimize the effect of heat losses and condensation of moisture at the walls. The partial top wall, which serves as a constant temperature heat sink, is multipass heat exchanger. Heat exchanger is connected through a valve system to constant temperature bath where the liquid nitrogen is used as the cooling medium. The distributions of temperature within the sample are measured using the thermocouples with a diameter of 0.15 mm. Thirty thermocouples are placed at the midplane of test cell (y =1.25 cm) in both horizontal and vertical directions (x–z plane) with longitudinal and transverse intervals of 10 mm. These thermocouples are connected to data logger and computer through which the temperatures could be measured and store at preselected time intervals. The positions of freezing front in the sample are determined by interpolating the fusion temperature from the thermocouple reading.

The uncertainty in the results might come from the variations in humidity, room temperature, and human error. The calculated uncertainty associated with temperature is less than 2.70%. The calculated uncertainties in all tests are less than 2.75%.

Results and Discussions

Validation Test. In order to verify the accuracy of the present numerical study, the present numerical algorithm was validated by performing simulations for a planar freezing front in a phase change slab (water) with a dimension of 10 cm(x)×5 cm(z). The initial temperature of 0°C is described throughout each layer. Thereafter, the constant temperature heat sink (T_L=−80°C) is imposed on the partial top wall. The results are compared with the analytical solution appeared in the classical paper [32], which is also commonly referred to in literature, for the freezing of a phase change slab (water) at the same condition. Figure 4 clearly shows a good agreement of the locations of freezing front. All of these favorable comparisons lend confidence in the accuracy of the numerical results of the present work.

Freezing Front Tracking Grid Generation System. To illustrate the efficiency of the grid generation system during the freezing of water in a rectangular cavity with a dimension of 10 cm(x)×5 cm(z) filled with a PM (porosity, ϕ=0.4) subjected to a constant temperature heat sink (single heat sink with strip length of 20 mm), the initial temperature of 0°C is described throughout each layer. Thereafter, the constant temperature heat sink (T_L=−40°C) is imposed on the partial top wall. The calcu-

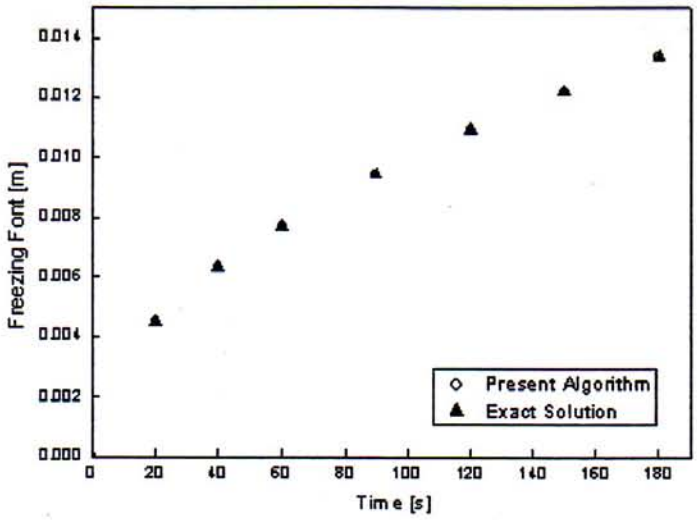

Fig. 4 Validation test for a planar freezing font in a phase-change slab

lated results are based on the thermal properties from Table 1.

In order to check the influence of numerical grid on the solutions, computations were carried out using 100×50 and 100×100 grids on entire computational domain, respectively. The results obtained from this study are presented in Fig. 5 in the form of an interface deformation (freezing front). It is obvious from the figure that with the present method, the overall interface deformation qualitatively remains the same for two different grids; however, the spreading of the melt in both directions in the first case (using 100×50 grids) is higher than the second case (using 100×100 grids). In addition, it is also evident that the solution was yet to reach a grid independent state. At this point, it may be mentioned here that the main objective of the present paper is not to demonstrate the features of phase change freezing problem but

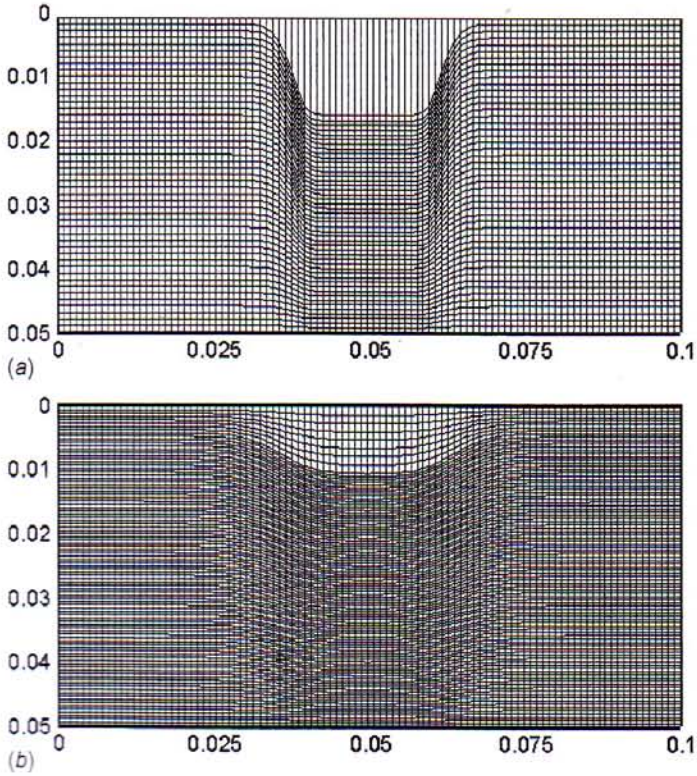

Fig. 5 The interface deformation in computational domain with different numerical grids: (*a*) 100×50 grids (*b*) 100×100 grids

to present novel numerical approach to solve phase change problem on a moving grids. Hence, no further study was carried out to obtain a grid independent solution and all the subsequent results are presented for 100×100 grid.

The following results (Figs. 6(*a*)–6(*f*) show grids that fit curves, which are the typical shapes seen during deformation of an interface with respect to elapsed times. Furthermore, the grids show significant variation of density and skewness along the interface. It can be seen that the location of freezing front is progressed with respect to elapsed times. During the initial stages of freezing, the shape of the interface in each region becomes flatter as the freezing front moves further away from the fixed boundary indicating principally 1D heat flow. As time progresses, the curve on the interface gradually beetles indicating the 2D effect.

Figure 7 shows the measured and simulated results of the freezing front during the freezing of water in a rectangular cavity (with a dimension of 10 cm(x) $\times$ 5 cm(z)) filled with a PM subjected to a constant temperature heat sink. In this comparison, the single constant temperature heat sink, $T_L=-40\,^{\circ}\mathrm{C}$, is applied. The observation of the freezing front depicted from the figure reveals that the simulated results and experimental results are qualitatively consistent. However, the experimental data are significantly lower than the simulated results. Discrepancy may be attributed to heat loss and nonuniform heating effect along the surface of supplied load. Numerically, the discrepancy may be attributed to uncertainties in the thermal and physical property data. In addition, the source of the discrepancy may be attributed to natural convection effect in liquid.

It is found that the grid is able to maintain a significant amount of orthogonality and smoothness both within the interior and along the boundary as the grid points redistributed themselves to follow the interface. These results show the efficiency of the present method for the moving boundary problem.

Freezing Process. The present work is to couple the grid generation algorithm with the transport equations. The thermal analysis during freezing process will be discussed in this section. The simulations of temperature distribution within rectangular cavity filled with porous media in the vertical plane ($x-z$) corresponding to grid simulating the deformation of an interface (Figs. 6(*a*)–6(*f*)) are shown in Figs. 8(*a*)–8(*f*)). Since the present work is to couple the grid generation algorithm with the transport equations, the thermal analysis during freezing process will be discussed as follows. When a constant temperature heat sink is applied during localized freezing process, heat is conducted from the hotter region in unfrozen layer to the cooler region in frozen layer. At the initial stages of freezing, the freezing fronts seem to be a square in shape indicating principally 1D heat flow, as explained for Figs. 6(*a*)–6(*f*). Later, the freezing fronts gradually exhibit a typical shape for 2D heat conduction dominated freezing. However, as the freezing process persists, the freezing rate progresses slowly. This is because most of heat conduction takes place the leading edge of frozen layer (freeze layer), which is located further from unfrozen layer. Consequently, small amount of heat can conduct to the frozen layer due to the freeze region acting as an insulator and causing freezing fronts to move slowly with respect to elapsed times. Considering the shapes of the freezing front with respect to elapsed times, each freezing region of the rectangular cavity shows signs of freezing, while the outer edge displays no obvious sign of freezing indicating that the temperature does not fall below $0\,^{\circ}\mathrm{C}$. Nevertheless, at the long stages of freezing, the spreading of the freeze in both the $x-z$ directions (semicircular shape) is clearly shown.

This study shows the capability of the present method to correctly handle the phase change problem. With further quantitative validation of the present method, this method can be used as a tool for investigating in detail this particular freezing of phase change slab at a fundamental level.

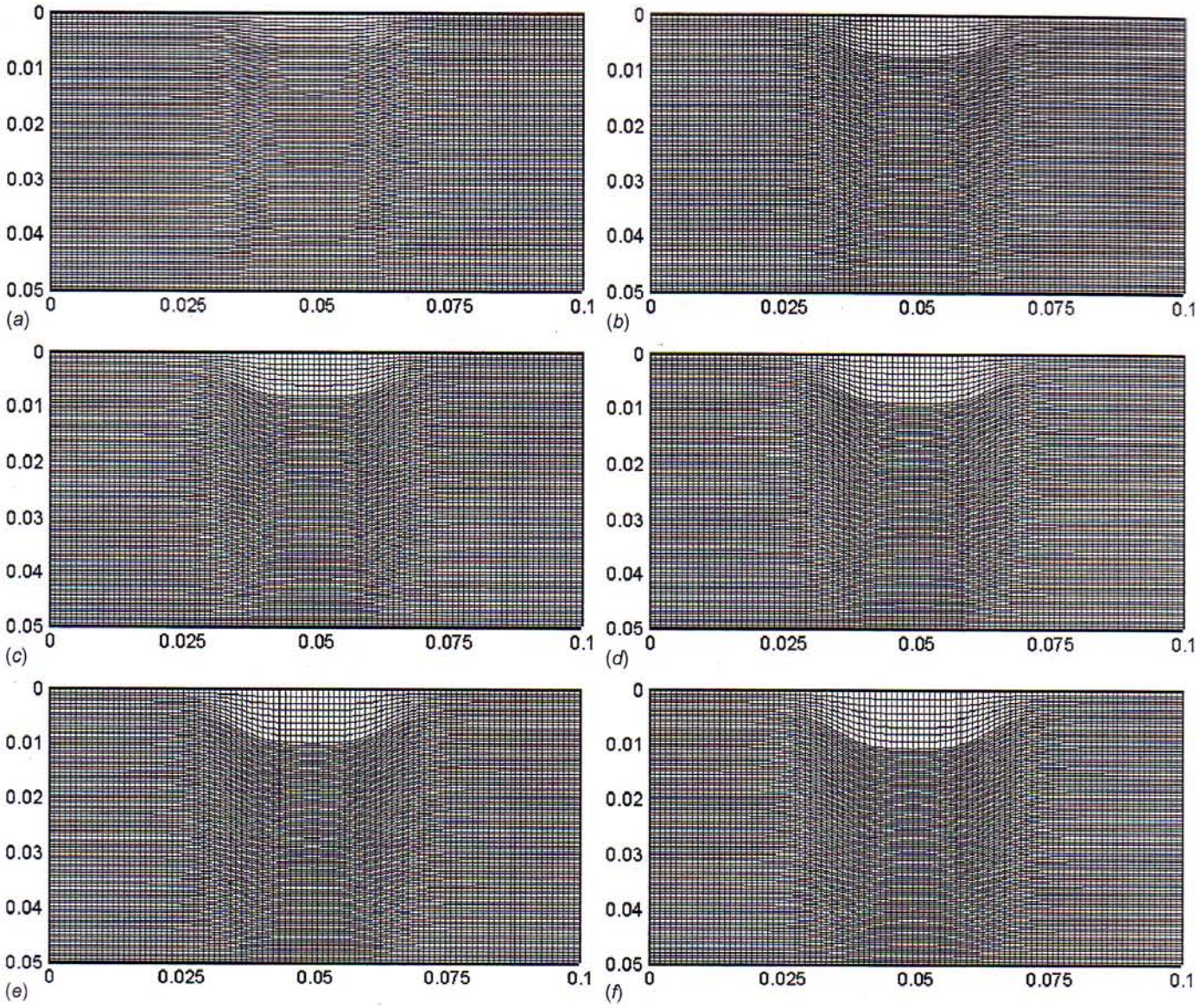

Fig. 6 Grid simulating the deformation of an interface: (*a*) freezing time of 30 s, (*b*) freezing time of 60 s, (*c*) freezing time of 90 s, (*d*) freezing time of 120 s, (*e*) freezing time of 150 s, and (*f*) freezing time of 180 s

Conclusions

Mesh quality has the largest impact on solution quality. A high quality mesh increases the accuracy of the computational flow solution and improves convergence. Therefore, it is important to provide tools for obtaining and improving a mesh.

In this study, the freezing of water in a rectangular cavity filled with a PM subjected to a constant temperature heat sink has been investigated numerically. A generalized mathematical model and an effective calculation procedure is proposed. A preliminary case study indicates the successful implementation of the numerical procedure. A two-dimensional freezing model is then validated against available analytical solutions and experimental results and subsequently used as a tool for efficient computational prototyping. Simulated results are in good agreement with available analytical solution and experimental results. The successful comparison with analytical solution and experiments should give confidence in the proposed mathematical treatment, and encourage the acceptance of this method as useful tool for exploring practical problems.

The next phase, which has already begun, is to couple the grid generation algorithm with the complete transport equations that determine the moving boundary front and buoyancy-driven convection in the unfrozen layer (liquid). Moreover, some experimental studies will be performed to validate numerical results.

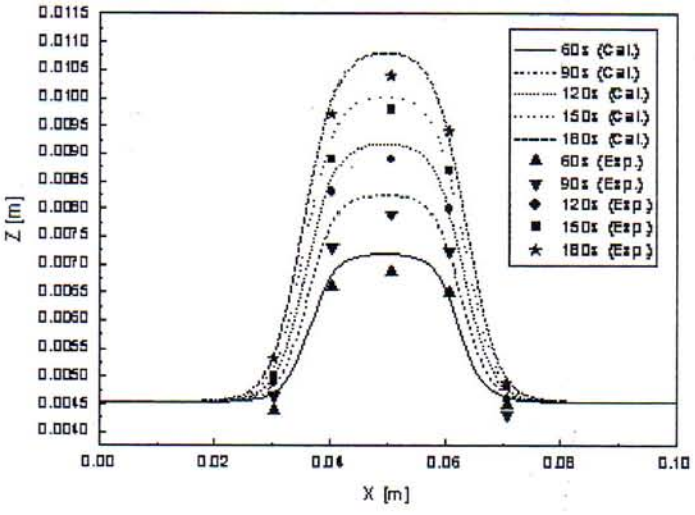

Fig. 7 Comparison of experimental data and simulated freezing front from present numerical study

Acknowledgments

The authors are pleased to acknowledge Thailand Research Fund for supporting this research work. Professor K. Aoki of the

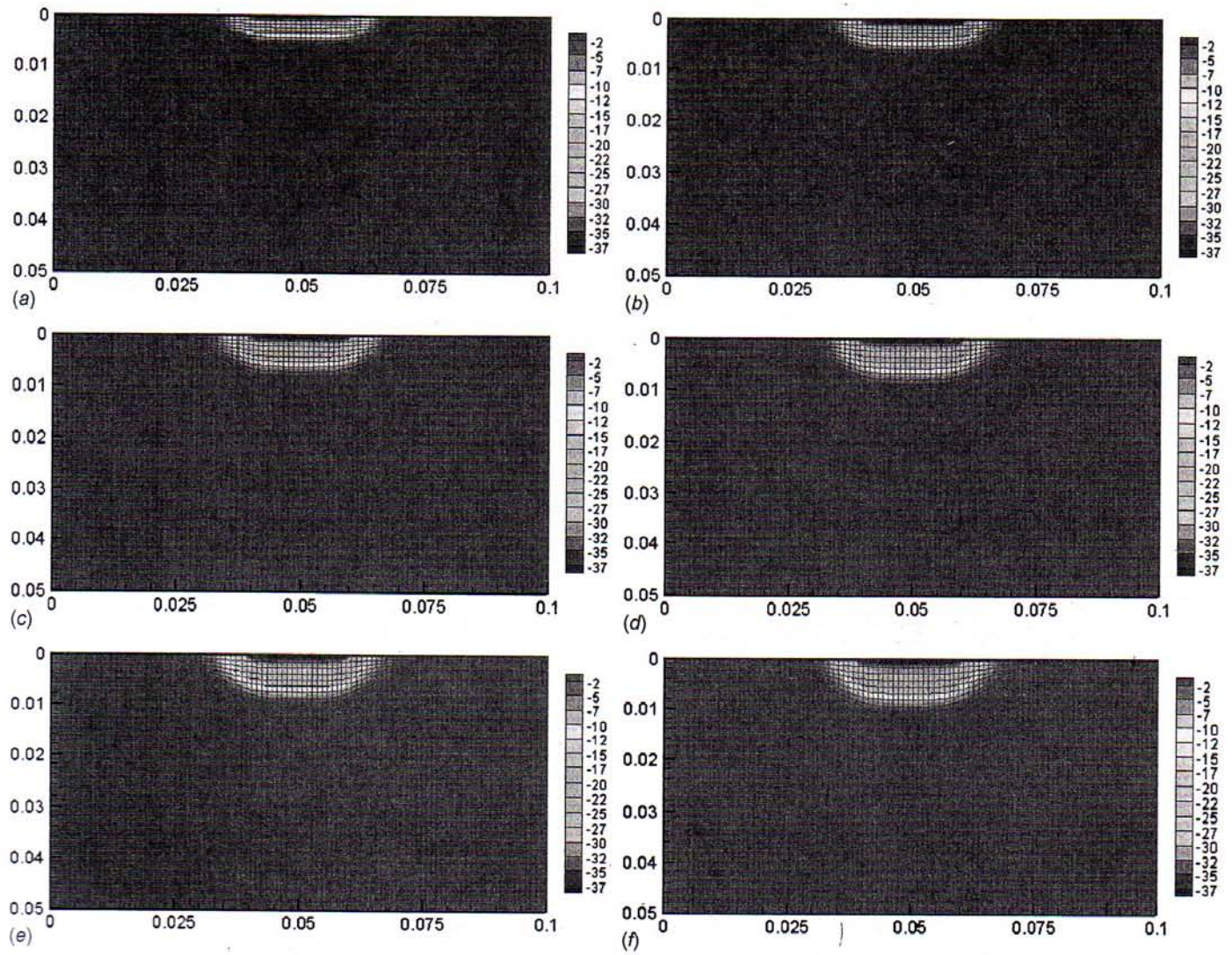

Fig. 8 The simulations of temperature distribution (Unit: °C): (*a*) freezing time of 30 s, (*b*) freezing time of 60 s, (*c*) freezing time of 90 s, (*d*) freezing time of 120 s, (*e*) freezing time of 150 s, and (*f*) freezing time of 180 s

Nagaoka University of Technology are also gratefully acknowledged for his valuable recommendations in this research area.

Nomenclature

a = thermal diffusivity (m^2/s)
C_p = specific heat capacity (J/kg K)
L = latent heat (J/kg)
T = temperature (°C)
t = time (s)
x, z = Cartesian coordinates
λ = effective thermal conductivity (W/mK)
ϕ = porosity

Subscripts

i = initial
f = fusion
j = layer number
l = unfrozen
s = frozen

Appendix

In this section, we will derive a transformation model of the governing differential equations for using in the numerical calculation. The details are shown below.

1 General Transformation of the First and Second Derivatives

Considering the first derivative of any parameters can be written as

$$\frac{\partial}{\partial x} = \frac{1}{J}\left(z_\eta \frac{\partial}{\partial \xi} - z_\xi \frac{\partial}{\partial \eta}\right)$$

$$\frac{\partial}{\partial z} = \frac{1}{J}\left(x_\xi \frac{\partial}{\partial \eta} - x_\eta \frac{\partial}{\partial \xi}\right) \tag{A1}$$

where J is Jacobian. It can be written as

$$J = x_\xi z_\eta - x_\eta z_\xi \tag{A2}$$

$$x_\xi = \frac{\partial x}{\partial \xi} \tag{A3}$$

Considering the second derivative of any parameters, we will establish the second derivative of Laplace equation of parameter A where Eqs. (A1) and (A3) are related:

$$\nabla^2 A = \left(\frac{\partial^2}{\partial x^2} + \frac{\partial^2}{\partial z^2}\right)A = \frac{1}{J^2}\left(\alpha\frac{\partial^2 A}{\partial \xi^2} - 2\beta\frac{\partial^2 A}{\partial \xi \partial \eta} + \gamma\frac{\partial^2 A}{\partial \eta^2}\right) + \frac{1}{J^3}\left[(\alpha x_{\xi\xi} - 2\beta x_{\xi\eta} + \gamma x_{\eta\eta})\left(z_\xi\frac{\partial A}{\partial \eta} - z_\eta\frac{\partial A}{\partial \xi}\right) + (\alpha z_{\xi\xi} - 2\beta z_{\xi\eta} + \gamma z_{\eta\eta})\times\left(x_\eta\frac{\partial A}{\partial \xi} - x_\xi\frac{\partial A}{\partial \eta}\right)\right] \quad \text{(A4)}$$

where

$$\alpha = x_\eta^2 + z_\eta^2$$

$$\beta = x_\xi x_\eta + z_\xi z_\eta$$

$$\gamma = x_\xi^2 + z_\xi^2 \quad \text{(A5)}$$

x_ξ, x_ξ, z_ξ, and z_η denote the partial derivatives, β, α, γ are the geometric factors, and η, ξ are the transformed coordinates. The related parameter can be defined as

$$x = x(\xi,\eta) \quad z = z(\xi,\eta) \text{ or } \xi = \xi(x,z) \quad \eta = \eta(x,z)$$

$$\Downarrow$$

$$x = x(\xi) \quad z = z(\xi,\eta) \text{ or } \xi = \xi(x) \quad \eta = \eta(x,z)$$

$$\therefore x_\eta = \frac{\partial x}{\partial \eta} = 0 \text{ or } \xi_x = \frac{\partial \xi}{\partial x} = 0 \quad \text{(A6)}$$

Corresponding to Eq. (A6), the first derivative of any parameters (Eq. (A1)) can be rewritten as

$$\frac{\partial}{\partial x} = \frac{1}{J}\left(z_\eta\frac{\partial}{\partial \xi} - z_\xi\frac{\partial}{\partial \eta}\right) \quad \frac{\partial}{\partial z} = \frac{1}{J}\left(x_\xi\frac{\partial}{\partial \eta} - x_\eta\frac{\partial}{\partial \xi}\right)$$

$$\Downarrow$$

$$\frac{\partial}{\partial x} = \frac{1}{J}\left(z_\eta\frac{\partial}{\partial \xi} - z_\xi\frac{\partial}{\partial \eta}\right) \quad \frac{\partial}{\partial z} = \frac{1}{J}\left(x_\xi\frac{\partial}{\partial \eta}\right) \quad \text{(A7)}$$

where

$$J = x_\xi z_\eta - x_\eta z_\xi$$

$$\Downarrow$$

$$J = x_\xi z_\eta \quad \text{(A8)}$$

The second derivative of any parameters (Eq. (A4)) can be also rewritten as

$$\nabla^2 A = \frac{1}{J^2}\left(\alpha\frac{\partial^2 A}{\partial \xi^2} - 2\beta\frac{\partial^2 A}{\partial \xi \partial \eta} + \gamma\frac{\partial^2 A}{\partial \eta^2}\right) + \frac{1}{J^3}\left[(\alpha x_{\xi\xi} - 2\beta x_{\xi\eta} + \gamma x_{\eta\eta})\times\left(z_\xi\frac{\partial A}{\partial \eta} - z_\eta\frac{\partial A}{\partial \xi}\right) + (\alpha z_{\xi\xi} - 2\beta z_{\xi\eta} + \gamma z_{\eta\eta})\left(x_\eta\frac{\partial A}{\partial \xi} - x_\xi\frac{\partial A}{\partial \eta}\right)\right]$$

$$\Downarrow$$

$$\nabla^2 A = \frac{1}{J^2}\left(\alpha\frac{\partial^2 A}{\partial \xi^2} - 2\beta\frac{\partial^2 A}{\partial \xi \partial \eta} + \gamma\frac{\partial^2 A}{\partial \eta^2}\right) + \frac{1}{J^3}\left[(\alpha x_{\xi\xi})\left(z_\xi\frac{\partial A}{\partial \eta} - z_\eta\frac{\partial A}{\partial \xi}\right) + (\alpha z_{\xi\xi} - 2\beta z_{\xi\eta} + \gamma z_{\eta\eta})\left(-x_\xi\frac{\partial A}{\partial \eta}\right)\right] \quad \text{(A9)}$$

where

$$\alpha = x_\eta^2 + z_\eta^2 \quad \beta = x_\xi x_\eta + z_\xi z_\eta \quad \gamma = x_\xi^2 + z_\xi^2$$

$$\Downarrow$$

$$\alpha = z_\eta^2 \quad \beta = z_\xi z_\eta \quad \gamma = x_\xi^2 + z_\xi^2 \quad \text{(A10)}$$

2 Transformation of Thermal Model

After some mathematical manipulations (Eqs. (A7), (A9), (3), and (4), and Eq. (5)), a transformation model of the governing differential equations becomes

$$\frac{\partial T_l}{\partial t} = \frac{a_l}{J^2}\left(\alpha\frac{\partial^2 T_l}{\partial \xi^2} - 2\beta\frac{\partial^2 T_j}{\partial \xi \partial \eta} + \gamma\frac{\partial^2 T_l}{\partial \eta^2}\right) + \frac{a_l}{J^3}\left[\left(\alpha\frac{\partial^2 x}{\partial \xi^2}\right)\left(z_\xi\frac{\partial T_l}{\partial \eta} - z_\eta\frac{\partial T_l}{\partial \xi}\right) + \alpha\frac{\partial^2 z}{\partial \xi^2} - 2\beta\frac{\partial^2 z}{\partial \xi \partial \eta} + \gamma\frac{\partial^2 z}{\partial \eta^2}\left(-x_\xi\frac{\partial T_l}{\partial \eta}\right)\right] + \frac{1}{J}\left(x_\xi\frac{\partial T_l}{\partial \eta}\right)\frac{dz}{dt} \quad \text{(A11)}$$

$$\frac{\partial T_s}{\partial t} = \frac{a_s}{J^2}\left(\alpha\frac{\partial^2 T_s}{\partial \xi^2} - 2\beta\frac{\partial^2 T_s}{\partial \xi \partial \eta} + \gamma\frac{\partial^2 T_s}{\partial \eta^2}\right) + \frac{a_s}{J^3}\left[\left(\alpha\frac{\partial^2 x}{\partial \xi^2}\right)\left(z_\xi\frac{\partial T_s}{\partial \eta} - z_\eta\frac{\partial T_s}{\partial \xi}\right) + \alpha\frac{\partial^2 z}{\partial \xi^2} - 2\beta\frac{\partial^2 z}{\partial \xi \partial \eta} + \gamma\frac{\partial^2 z}{\partial \eta^2}\left(-x_\xi\frac{\partial T_s}{\partial \eta}\right)\right] + \frac{1}{J}\left(x_\xi\frac{\partial T_s}{\partial \eta}\right)\frac{dz}{dt} \quad \text{(A12)}$$

$$\left[\lambda_s\frac{1}{J}\left(x_\xi\frac{\partial T_s}{\partial \eta}\right) - \lambda_l\frac{1}{J}\left(x_\xi\frac{\partial T_l}{\partial \eta}\right)\right]\left\{1 + \left[\frac{1}{J}\left(z_\eta\frac{\partial z_{\text{mov}}}{\partial \xi} - z_\xi\frac{\partial z_{\text{mov}}}{\partial \eta}\right)\right]^2\right\} = \rho_s L_s\frac{\partial z_{\text{mov}}}{\partial t} \quad \text{(A13)}$$

References

[1] Landua, H. G., 1950, "Heat Conduction in a Melting Solid," Q. Appl. Math., **8**, pp. 81–94.

[2] Murray, W. D., and Landis, F., 1959, "Numerical and Machine Solutions of Transient Heat Conduction Problem Involving Melting or Freezing," ASME J. Heat Transfer, **81**, pp. 106–112.

[3] Frivik, P. E., and Comini, G., 1982, "Seepage and Heat Flow in Soil Freezing," ASME J. Heat Transfer, **104**, pp. 323–328.

[4] Sparrow, E. M., and Broadbent, J. A., 1983, "Freezing in a Vertical Tube," ASME J. Heat Transfer, **105**, pp. 217–225.

[5] Voller, V., and Cross, M., 1981, "Accurate Solutions of Moving Boundary Problems Using the Enthalpy Method," Int. J. Heat Mass Transfer, **24**, pp. 545–556.

[6] Weaver, J. A., and Viskanta, R., 1986, "Freezing of Liquid-Saturated Porous Media," ASME J. Heat Transfer, **108**, pp. 654–659.

[7] Chellaiah, S., and Viskanta, R., 1988, "Freezing of Saturated and Superheated Liquid in Porous Media," Int. J. Heat Mass Transfer, **31**, pp. 321–330.

[8] Hasan, M., Mujumdar, A. S., and Weber, M. E., 1991, "Cyclic Melting and Freezing," Chem. Eng. Sci., **46**(7), pp. 1573–1587.

[9] Charn-Jung, K., and Kaviany, M., 1992, "Numerical Method for Phase-Change Problems with Convection and Diffusion," Int. J. Heat Mass Transfer, **35**(2), pp. 457–467.

[10] Rattanadecho, P., 2004, "Experimental and Numerical Study of Solidification Process in Unsaturated Granular Packed Bed," J. Thermophys. Heat Transfer, **18**(1), pp. 87–93.

[11] Rattanadecho, P., 2004, "The Theoretical and Experimental Investigation of Microwave Thawing of Frozen Layer Using Microwave Oven (Effects of Layered Configurations and Layered Thickness)," Int. J. Heat Mass Transfer, **47**(5), pp. 937–945.

[12] Pak, J., and Plumb, O. A., 1997, "Melting in a Two-Component Packed Bed," ASME J. Heat Transfer, **119**(3), pp. 553–559.

[13] Hao, Y. L., and Tao, Y.-X., 2001, "Melting of a Solid Sphere Under Forced and Mixed Convection: Flow Characteristics," ASME J. Heat Transfer, **123**(5), pp. 937—950.

[14] Attinger, D., and Poulikakos, D., 2001, "Melting and Resolidification of a Substrate Caused by Molten Microdroplet Impact," ASME J. Heat Transfer, **123**(6), pp. 1110–1122.

[15] Jiang, J., Hao, Y., and Tao, Y.-X., 2002, "Experimental Investigation of Convective Melting of Granular Packed Bed Under Microgravity," ASME J. Heat Transfer, **124**(3), pp. 516–524.

[16] Hao, Y. L., and Tao, Y.-X., 2002, "Heat Transfer Characteristics of Melting Ice Spheres Under Forced and Mixed Convection," ASME J. Heat Transfer, **124**(5), pp. 891–903.

[17] Elgafy, A., Mesalhy, O., and Lafdi, K., 2004, "Numerical and Experimental Investigations of Melting and Solidification Processes of High Melting Point PCM in a Cylindrical Enclosure," ASME J. Heat Transfer, **126**(5), pp. 869–875.

[18] Ayasoufi, A., Keith, T. G., and Rahmani, R. K., 2004, "Application of the Conservation Element and Solution Element Method in Numerical Modeling

of Three-Dimensional Heat Conduction With Melting and/or Freezing," ASME J. Heat Transfer, **126**(6), pp. 937–945.

[19] Lynch, D. R., 1982, "Unified Approach to Simulation on Deforming Elements With Application to Phase Change Problem," J. Comput. Phys., **47**, pp. 387–441.

[20] Cao, W., Huang, W., and Russell, R. D., 1999, "An r-Adaptive Finite Element Method Based Upon Moving Mesh PDEs," J. Comput. Phys., **149**, pp. 221–244.

[21] Chatterjee, A., and Prasad, V., 2000, "A Full 3-Dimensional Adaptive Finite Volume Scheme for Transport and Phase-Change Processes, Part I: Formulation and Validation," Numer. Heat Transfer, Part A, **37**(8), pp. 801–821.

[22] Duda, J. L., Malone, M. F., Notter, R. H., and Vrentas, J. S., 1975, "Analysis of Two-Dimensional Diffusion Controlled Moving Boundary Problems," Int. J. Heat Mass Transfer, **18**, pp. 901–910.

[23] Saitoh, T., 1978, "Numerical Method for Multi-Dimensional Freezing Problems in Arbitrary Domains," ASME J. Heat Transfer, **100**, pp. 294–299.

[24] Gong, Z.-X., and Mujumdar, A. S., 1998, "Flow and Heat Transfer in Convection-Dominated Melting in a Rectangular Cavity Heated From Below," Int. J. Heat Mass Transfer, **41**(17), pp. 2573–2580.

[25] Beckett, G., MacKenzie, J. A., and Robertson, M. L., 2001, "A Moving Mesh Finite Element Method for the Solution of Two-Dimensional Stefan Problems," J. Comput. Phys., **168**(2), pp. 500–518.

[26] Eriksson, L. E., 1982, "Generation of Boundary-Conforming Grid Around Wing-Body Configurations Using Transfinite Interpolation," AIAA J., **20**, pp. 1313–1320.

[27] Coons, S. A., 1967, "Surfaces for Computer-Aided Design of Space Forms," Project MAC, Technical Report MAC-TR 44 MIT.

[28] Cook, W. A., 1974, "Body Oriented Coordinates for Generating 3-Dimensional Meshes," Int. J. Numer. Methods Eng., **8**, pp. 27–43.

[29] Gordon, W. J., and Hall, C. A., 1973, "Construction of Curvilinear Coordinate Systems and Applications to Mesh Generation," Int. J. Numer. Methods Eng., **7**, pp. 461–477.

[30] Ettouney, H. M., and Brown, R. A., 1983, "Finite-Element Methods for Steady Solidification Problems," J. Comput. Phys., **49**, pp. 118–150.

[31] Anderson, J. D., 1995, Computational Fluid Dynamics, Int. Ed., McGraw-Hill, New York, Chap. 5.

[32] Yao, L. S., and Prusa, J., 1990, "Melting and Freezing," Adv. Heat Transfer, **19**, pp. 1–95.